Materials and Design 56 (2014) 165–173

Contents lists available at ScienceDirect

Materials and Design

journal homepage: www.elsevier.com/locate/matdes

Study on cold metal transfer welding–brazing of titanium to copper

R. Cao *, Z. Feng, Q. Lin, J.H. Chen *

State Key Laboratory of Gansu Advanced Non-ferrous Metal Materials, Lanzhou University of Technology, Lanzhou 730050, PR China
Key Laboratory of Non-ferrous Metal Alloys of Ministry of Education, Lanzhou University of Technology, Lanzhou 730050, PR China

ARTICLE INFO

Article history:
Received 8 August 2013
Accepted 17 October 2013
Available online 28 October 2013

Keywords:
Titanium
Copper
Cold metal transfer
Welding–brazing
Butt joint
Intermetallic compounds

ABSTRACT

3 mm Pure titanium TA2 was joined to 3 mm pure copper T2 by Cold Metal Transfer (CMT) welding–brazing process in the form of butt joint with a 1.2 mm diameter ERCuNiAl copper wire. The welding–brazing joint between Ti and Cu base metals is composed of Cu–Cu welding joint and Cu–Ti brazing joint. Cu–Cu welding joint can be formed between the Cu weld metal and the Cu groove surface, and the Cu–Ti brazing interface can be formed between Cu weld metal and Ti groove surface. The microstructure and the intermetallic compounds distribution were observed and analyzed in details. Interfacial reaction layers of brazing joint were composed of Ti_2Cu, TiCu and $AlCu_2Ti$. Furthermore, crystallization behavior of welding joint and bonding mechanism of brazing interfacial reaction were also discussed. The effects of wire feed speed and groove angle on the joint features and mechanical properties of the joints were investigated. Three different fracture modes were observed: at the Cu interface, the Ti interface, and the Cu heat affected zone (HAZ). The joints fractured at the Cu HAZ had higher tensile load than the others. The lower tensile load fractured at the Cu interface or Ti interface was attributed to the weaker bonding degree at the Cu interface or Ti interface.

1. Introduction

Hybrid structures of dissimilar metals have been gradually appreciated in national defense and civil industrial fields, such as aerospace, shipbuilding, energy and electric power industry [1]. Hybrid structure of Ti/Cu dissimilar alloys not only satisfies the requirements of heat conduction, electrical conduction, wear resistance and corrosion resistance, but also meets demand of light weight and high strength. However, fusion joining of titanium and copper has a metallurgical challenge because of the great differences in their chemical and physical properties, and mass of brittle Ti–Cu intermetallic compounds (IMCs) are formed at elevated temperatures seriously degrading the mechanical properties of the joints [2–6]. It is necessary to control effectively formation and growth of Ti–Cu IMCs. Solid-state welding methods, e.g. explosive welding and friction welding, have been used to make Ti/Cu dissimilar metals joint, but the shape and size of such solid-state joints are extremely restricted [7–9].

In recent years, welding–brazing methods have been developed for dissimilar metals with large difference in melting point, e.g. tungsten inert gas (TIG) arc welding–brazing of Al to steel [10,11], laser welding–brazing of Ti to Al [12] and electron beam self-melting brazing of Ti to Cu [13]. In the welding–brazing process, the metal with low melting point and filler metals were molten and mixed to form a fusion welding joint, the metal with high melting point was little molten or maintain solid, and the liquid filler metal wetted and spread on the metal with high melting point to form a brazing joint.

Nowadays, Cold metal transfer (CMT) process is a new technique and becomes a hot research field in dissimilar materials welding [14,15]. CMT welding–brazing of Al to steel [16,17], CMT welding–brazing of Al to Ti [18] have been carried out in recent years. In this study, commercially pure titanium TA2 and commercially pure copper T2 were joined using a 1.2 mm diameter ERCuNiAl (AWS A5.7/A5.7 M) copper wire through CMT welding–brazing. Ti/Cu CMT welding–brazing butt joint was composed of Cu–Cu welding joint in the Cu side and Cu–Ti brazing joint in the Ti side. Three different configurations of Cu/Ti butt joints with various welding bevel grooves were adopted. The influence of different groove angles of Cu side and wire feed speed on the features and mechanical properties of the joint were investigated. After welding, the weld appearance, tensile load, crystallization behavior and bonding mechanism of joints were analyzed and discussed.

2. Experimental details

2.1. Materials

The materials used in the study include 3 mm thick commercially pure titanium TA2 sheet and 3 mm thick commercially pure

* Corresponding authors at: Key Laboratory of Non-ferrous Metal Alloys of Ministry of Education, Lanzhou University of Technology, Lanzhou 730050, PR China. Tel.: +86 931 2973529; fax: +86 931 2976578.
E-mail addresses: caorui@lut.cn (R. Cao), zchen@lut.cn (J.H. Chen).

0261-3069/$ - see front matter © 2013 Elsevier Ltd. All rights reserved.
http://dx.doi.org/10.1016/j.matdes.2013.10.044

copper T2 sheet. The corresponded compositions, per the manufacturer's data sheet, are given in Table 1. Copper wire ERCuNiAl (AWS A5.7/A5.7 M) having a diameter of 1.2 mm was used in this study. Its chemical composition is shown in Table 2.

2.2. Welding procedure

The Ti and Cu sheets were machined to rectangular strips of 100 mm × 50 mm × 3 mm and designed as the butt joint configuration, as shown in Fig. 1. The V shape grooves with different groove angles were machined from the base metals. Three different configurations of Cu/Ti butt joints (*joint I* (Cu–T2–60°, Ti–TA2–30°), *joint II* (Cu–T2–45°, Ti–TA2–30°), *joint III* (Cu–T2–30°, Ti–TA2–30°)) with various groove angles were adopted in the experiments. In order to control effectively formation and growth of Ti–Cu IMCs and decrease the molten titanium, the wire was deviated from the edge of Cu sheet edge, as shown in Fig. 1.

The two sheets were degreased by acetone and polished by abrasive cloth first. Ti sheets were cleaned with HF 5% + HNO_3 35% aqueous solution for 10–20 min, then wiped and rinsed with ethanol and tap water. And the Cu sheets were wiped and rinsed with ethanol and tap water.

The CMT welding–brazing joining was carried out using TPS-3200 type CMT welding procedure. The welding parameters were listed as follows: welding speed (v_w) of 6 mm/s, wire feed speed (v_f) of 7.0–9.5 m/min, welding current (I_w) of 158–223 A, welding voltage (V_w) of 14.7–20.3 V, 99.99% argon shielding gas flow rate of 17 L/min. The various welding variables and the mechanical properties of Ti/Cu CMT butt joints were given in Table 3.

2.3. Characterization methods

After welding, in order to investigate the mechanical properties of the Ti/Cu CMT butt joints, tensile tests were carried out according to ISO 4136-2012 [19]. Three or two tensile specimens depicted in Fig. 2 were cut off from each weldment and tested on a WDW-100E type universal testing machine at the tensile speed of 1 mm/min at room temperature. Average tensile load of tensile specimens was taken to estimate the mechanical property of the joint.

According to ISO 9015-1: 2001 [20], the Vickers micro-hardness of the Ti/Cu butt joints was measured by the HX-1000 micro-hardness testing machine with a load of 200 gf for 5 s.

To study the microstructure and bonding mechanism of Ti/Cu CMT butt joint, the cross-sections of the specimens were prepared and examined. The microstructures of the welded joints and the IMCs were observed and analyzed by scanning electron microscope (i.e., Quanta FEG-450) equipped with energy dispersive X-ray spectrometer (EDS).

3. Results

3.1. Effects of wire feed speed and groove angle on the joint features

Fig. 3 shows the macroscopic cross-sections of three types of Ti/Cu CMT butt joints with different welding parameters listed in Table 3. For *joint I* (Cu–T2–60°, Ti–TA2–30°), at the v_f of 7.0 m/min and 8.0 m/min (I_w of 158 A and 184 A), the Cu base metal near Cu groove surface was not molten due to the low weld heat input

Table 2
Nominal chemical composition of ERCuNiAl copper wire (wt.%).

Alloy	Al	Ni	Pb	Fe	Mn	Cu
ERCuNiAl	8.0	6.0	0.038	3.0	1.0	Bal.

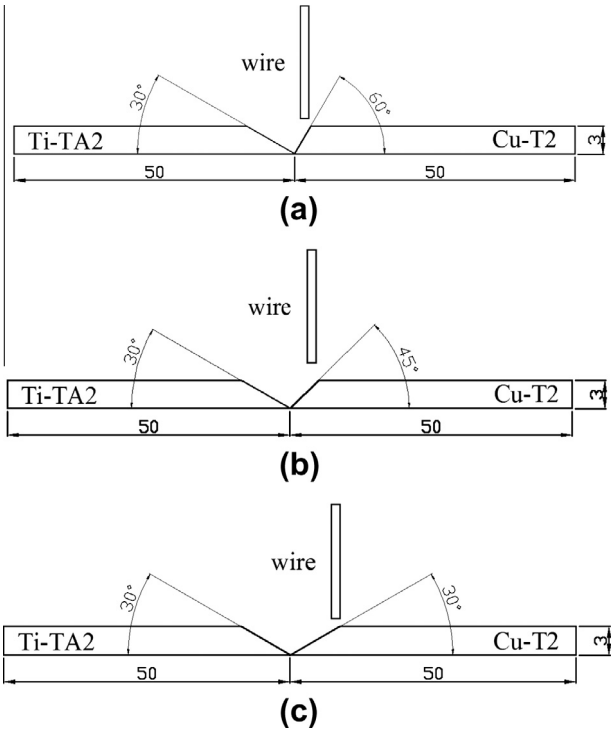

Fig. 1. Schematic diagram of Ti/Cu CMT butt joint: (a) *joint I* (Cu–T2–60°, Ti–TA2–30°), (b) *joint II* (Cu–T2–45°, Ti–TA2–30°), and (c) *joint III* (Cu–T2–30°, Ti–TA2–30°) (mm).

and the high thermal conductivity coefficient of copper (359.2 $Wm^{-1}K^{-1}$ [21]). For these low weld heat input, welding joint cannot be formed at the Cu groove side. However, the Cu–Ti interface between the liquid filler metal and the Ti groove surface can be successfully brazed, as shown in Fig. 3(a_0) and (b_0). Increasing the v_f to 9.0 m/min (I_w = 210 A), the welding–brazing joint was formed except only the root part of the Cu groove which was not fully molten, as shown in Fig. 3(c_0). At the high v_f of 9.5 m/min (I_w = 223 A), the excellent joint was formed as shown in Fig. 3(d_0). Based on Fig. 3(a_1–d_1), it was found that the formation process of *joint II* with groove angle of (T2–45°, TA2–30°) was similar to that of the *joint I*. But for *joint III* with lower groove angle on Cu side (T2–30°, TA2–30°), even at the low v_f of 7.0 m/min and 8.0 m/min (I_w of 158 A and 184 A), the liquid filler metal spread on the Cu groove surface to form the Cu–Cu weld metal. However, it still incompletely spread on the Ti groove surface, as shown in Fig. 3(a_2) and (b_2). Increasing the v_f to 9.0 m/min (I_w = 210 A), Ti groove surface was wetted by the molten Cu metal, yet the root region of the Cu groove was still incompletely molten, as shown in Fig. 3(c_2). Further increasing the v_f to 9.5 m/min (I_w = 223 A), the liquid filler metal spread on the Cu groove surface, and mixed with molten Cu

Table 1
Nominal chemical compositions of commercially pure titanium TA2 and commercially pure copper T2 (wt.%).

Materials	Bi	Pb	Fe	Mn	C	N	S	P	O	H	Ti	Cu
TA2	–	–	0.30	–	0.10	0.05	–	–	0.25	0.0015	Bal.	–
T2	0.002	0.005	–	–	–	–	0.005	0.03	–	–	–	Bal.

Table 3
Welding variables and mechanical properties of Ti/Cu CMT butt joints.

Joint type	Specimen No.	Wire feed speed (m/min)	Welding voltage (*V*)	Welding current (*A*)	Tensile load (kN)	Fracture modes
Joint I (Cu–T2–60°, Ti–TA2–30°)	1	7.0	14.7	158	0.95 (0.46, 0.68, 1.70)	Cu interface
	2	8.0	17.0	184	2.14 (1.66, 2.62)	Cu interface
	3	9.0	19.4	210	4.99 (4.92, 5.08, 4.98)	Cu-HAZ
	4	9.5	20.3	223	5.07 (4.92, 5.16, 5.12)	Cu-HAZ
Joint II (Cu–T2–45°, Ti–TA2–30°)	5	7.0	14.7	158	4.48 (4.86, 4.10)	Cu interface
	6	8.0	17.0	184	4.83 (5.16, 4.48, 4.84)	Cu-HAZ
	7	9.0	19.4	210	5.03 (5.16, 4.90, 5.04)	Cu-HAZ
	8	9.5	20.3	223	4.87 (4.92, 4.84, 4.86)	Cu-HAZ
Joint III (Cu–T2–30°, Ti–TA2–30°)	9	7.0	14.7	158	2.99 (2.74, 3.24)	Ti interface
	10	8.0	17.0	184	4.09 (3.60, 4.58)	Ti interface
	11	9.0	19.4	210	4.91 (4.80, 4.98, 4.96)	Cu-HAZ
	12	9.5	20.3	223	5.10 (5.10, 5.14, 5.06)	Cu-HAZ

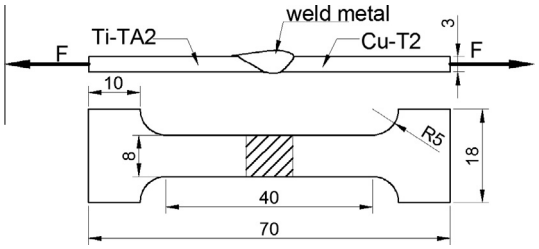

Fig. 2. The geometry of the tensile test samples (mm).

base metal, to form the Cu–Cu welding joint. Moreover, the liquid filler metal wetted and spread on the Ti groove surface, i.e. the Cu–Ti brazing interface was formed, as shown in Fig. 3(d_2).

Finally a fusion welding joint is formed in the Cu side. At the same time, liquid mixed metal interacts with Ti alloy in solid state, and a brazing joint is formed in the Ti side. Therefore, Ti/Cu CMT welding–brazing butt joint has dual characteristics of fusion welding and brazing.

In summary, the larger groove angle makes the fully melt of Cu difficult. The high welding current will be used to make fully molten and wetted welding–brazing joint.

3.2. Effects of wire feed speed and groove angle on the mechanical properties of the joint

In order to evaluate the mechanical property of the Ti/Cu CMT butt joints, tensile tests were conducted according to ISO 4136-2012 [19]. And the results were also given in Table 3. Fig. 4 shows

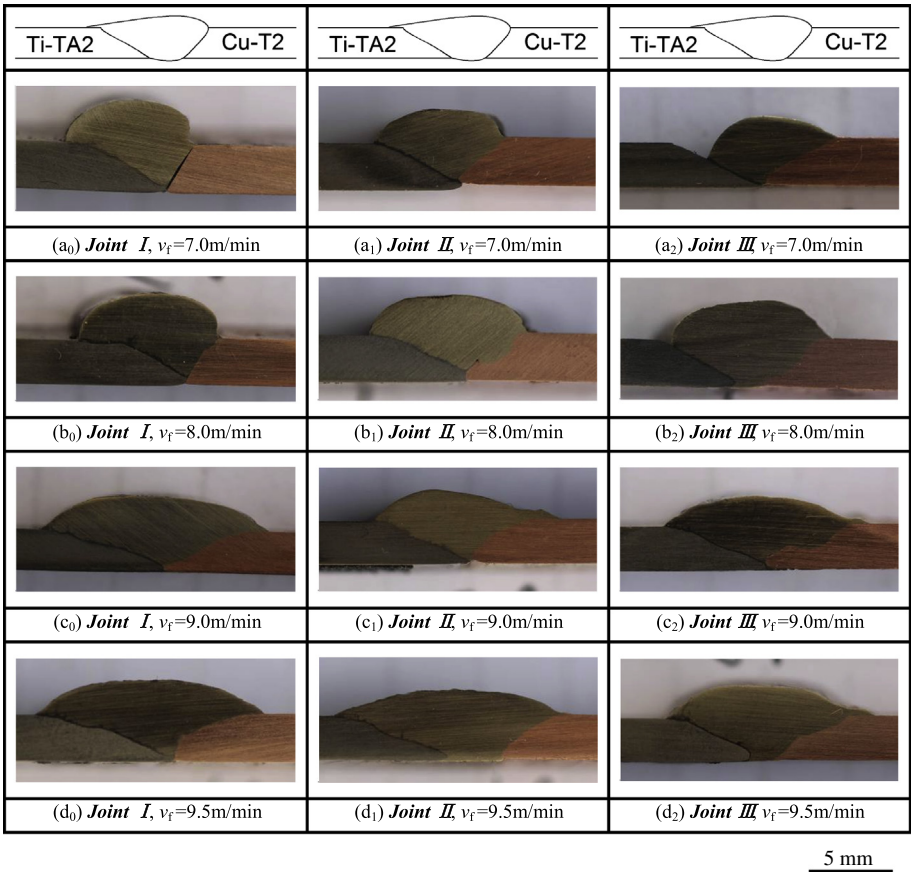

Fig. 3. Macroscopic cross section of the Ti/Cu CMT butt joints in different welding variables listed in Table 3.

the effects of the wire feed speed and the weld heat input on the tensile load. Fig. 5 presents the fracture modes of the joints after tensile test. Combined Fig. 4 and Table 3, it indicates that the tensile load increases with the increasing of the weld heat input (wire feed speed). For example, *joint I* and *joint II* with low weld heat input (wire feed speed) were fractured at the Cu interface with lower tensile load (as shown in Fig. 5(a)) due to un-fully molten Cu at Cu groove surface. For *joint III* with low groove angles of 30° on Cu side, the Cu base metal was fully molten. In this case, at low weld heat input (wire feed speed), the joint was fractured at the Ti brazing interface (see Fig. 5(b)) because the liquid filler metal incompletely spreading on the Ti groove surface produces weaker bonding at the Ti side. However, with the weld heat input increasing, the fracture locations of the joints were moved to the Cu HAZ with plastic fracture mode.

Comparing the weld appearance and mechanical properties, to join Ti and Cu at the larger range of welding variables, the *joint II* (T2–45°, TA2–30°) is the best choice. However, no matter which groove is designed, such as *joint I*, *joint II* or *joint III*, only if wire feed speed is controlled in range of 9.0–9.5 m/min (I_w = 210–223 A), the satisfied weld appearance and tensile load can be achieved. In these cases, the corresponded joint with high strength is fractured at the Cu HAZ.

In short, to obtain satisfied weld appearance and tensile strength, enough volume of weld metal should be produced. So, the principle to choose various groove angles and corresponded welding variables should guarantee to produce enough weld metal making satisfied joining between weld metal and Ti sheet, and satisfied joining between weld metal and Cu sheet.

In order to analyze the reason why higher strength is obtained in some specimens fractured in the Cu HAZ, according to ISO 9015-1: 2001 [20], the micro-hardness measurement was carried out on the HX-1000 micro-hardness testing machine along titanium base metal, weld metal zone to copper base metal for specimen #12 in Table 3. The results are shown in Fig. 6. Obviously, it is found that the hardness in the Cu HAZ with 9 mm width is lower than that of Cu base metal, i.e. the soften phenomena appear in the Cu HAZ. The result also shows that the micro-hardness of titanium base metal and weld metal are about 175 HV and 170 HV, respectively. However, the brazing interface zone reaches a micro-hardness of 500 HV. Tetsui [22] also found that a variety of IMCs of Ti and Cu formed near the brazing zone endowed its high hardness.

Based on the results, at the proper weld heat input (i.e., 680–754 J/mm, wire feed speed 9.0–9.5 m/min (I_w = 210–223 A)), the Ti/Cu CMT butt joint has tensile load of 5.10 kN, and fractures in the Cu HAZ during tensile test. The reason is attributed to the increasing of the strengths of Cu interface and Ti interface and the soften of Cu HAZ with increasing of weld heat input. During the CMT welding–brazing process, dynamic recrystallizations are done and crystalline grains grow rapidly at the Cu HAZ, resulting in the serious softening phenomena of Cu HAZ [8,23].

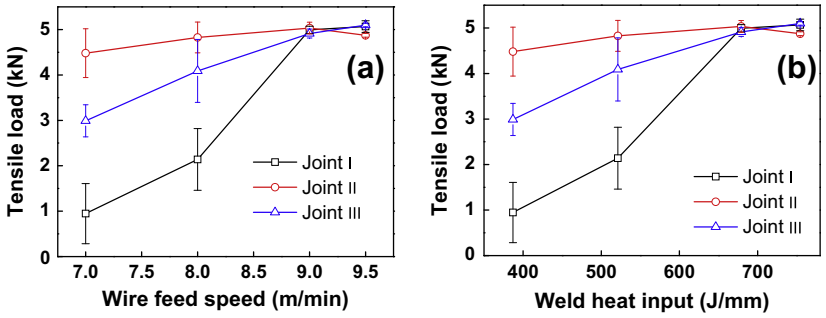

Fig. 4. The tensile load of Ti/Cu CMT butt joints in different welding variables listed in Table 3: (a) Effects of the wire feed speed on the tensile load, and (b) effects of the weld heat input on the tensile load.

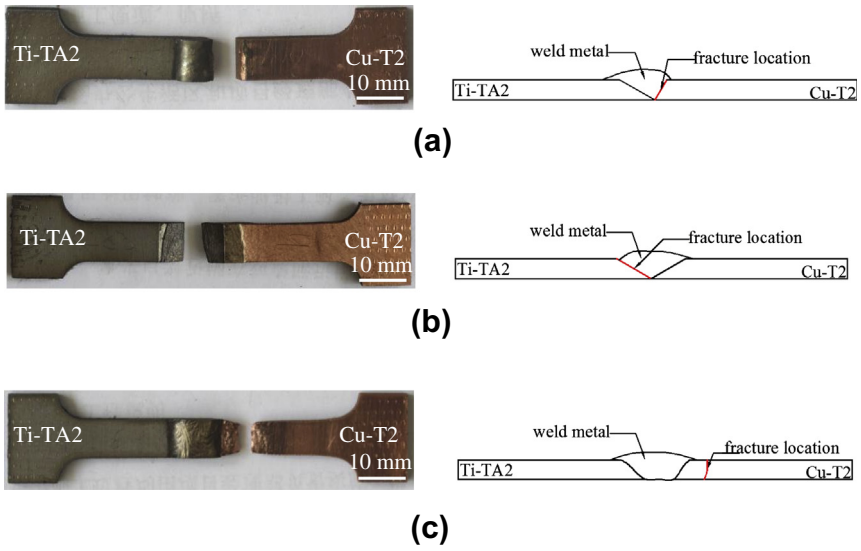

Fig. 5. Fracture modes of the joints: (a) the Cu interface, (b) the Ti interface, and (c) Cu HAZ.

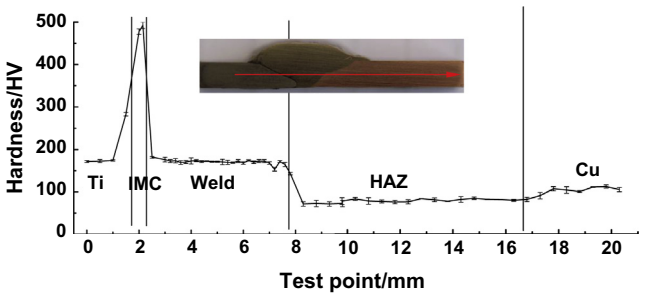

Fig. 6. Micro hardness of Ti/Cu CMT butt joint along the red line in macro cross section subfigure. (For interpretation of the references to colour in this figure legend, the reader is referred to the web version of this article.)

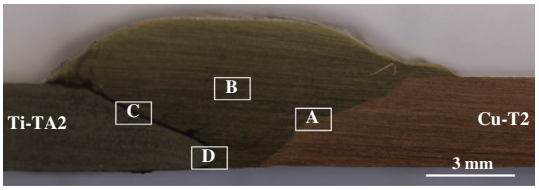

Fig. 8. Macroscopic cross-section of the Ti/Cu CMT butt *joint III* (Cu–T2–30, Ti–TA2–30) at the wire feed speed of 9.5 m/min.

3.3. Microstructure and bonding mechanism of the optimized Ti/Cu CMT welding–brazing butt joint

Fig. 7 shows weld appearance of the Ti/Cu CMT butt *joint III* (T2–30°, TA2–30°) with highest strength at the wire feed speed of 9.5 m/min. As shown in Fig. 7, the Ti/Cu CMT welding–brazing butt joint has a good front and back appearance. The molten ERCuNiAl copper filler metal had fully spread on the Ti surface, and no cracks appear on surface of welded joint at this heat input. Fig. 8 shows the macroscopic cross-section of Ti/Cu CMT welding–brazing butt joint indicated by a white dotted line location in Fig. 7(a).

Fig. 9(a) shows the magnified features of fusion zone (region A in Fig. 8), part of Cu base metal was molten and mixed with filler metal. In solidification, the solidified molten metal was nucleated on the fusion line between weld metal and Cu base metal and grew up quickly in cylindrical-like style. Fig. 9(b) shows the microstructures of weld metal (region B in Fig. 8), which are composed of α-Cu solid solutions (denoted by arrow 1) and Cu–Al–Ti–Fe–Ni multiphase (denoted by arrow 2). The compositions of these regions were listed in Table 4.

Figs. 10 and 11 show the SEM microstructures of brazing interface. Fig. 10 shows the magnified features of the brazing interface at the middle part of the groove surface (region C in Fig. 8). From Fig. 10(a), it is found that the IMCs layer thickness of the brazing interface at middle groove surface was about 117–129 μm. Fig. 10(b) presents higher magnification of zone C. According to their different morphological characteristics, the zone C could be divided into two reaction zones, which were marked as zone E close to Ti base metal and zone F next to the weld metal. The compositions of each zone (denoted by number 1–7 in Fig. 10) were analyzed by SEM–EDS. Based on the Ti–Cu binary phase diagram [24] and Ti–Cu–Al ternary phase diagram [25], the results were analyzed and listed in Table 5. Fig. 10(c) shows the microstructure of zone E (marked in Fig. 10(b)) near Ti base metal. The zone E consisted of gray Ti_2Cu phase (denoted by region 1) growing from the titanium base metal, big blocky TiCu phase (denoted by region 2) and white α-Cu solid solution (denoted by arrow 3). Fig. 10(d) shows the microstructure of zone F (marked in Fig. 10(b)) near to weld metal. Zone F contained gray Ti_2Cu phase (denoted by arrow 4), big blocky TiCu phase (denoted by arrow 5), big gray blocky $AlCu_2Ti$ phase (denoted by arrow 6) and white base α-Cu solid solution (denoted by arrow 7). Thus, the brazing interface mainly consisted of Ti_2Cu, TiCu and $AlCu_2Ti$ orderly from the Ti base metal to the weld metal. The results obtained in this study were in agreement with the previously published results [2–5].

Fig. 11 shows the magnified features of the brazing interface at root groove surface (region D in Fig. 8). As shown in Fig. 11(a), it is found the IMCs layer thickness of the brazing interface at root groove surface was about 80–100 μm. The SEM–EDS results were given in Table 6. From Fig. 11 and Table 6, the bonding microstructure of the brazing interface zone D is similar to that of brazing interface zone C. It can be seen that the general macro-features and microstructures are similar, but the thickness of the IMCs layers in different locations is different due to their various temperature gradient and interfacial reaction time during the brazing process.

In order to confirm the distribution of elements Ti, Cu and Al at the brazing interface, the SEM–EDS line analysis were carried out, as shown in Fig. 12. As seen, from the Ti base metal to the weld metal, the content of Cu element increases gradually while the content of Ti decreases gradually as a whole, and the distribution of elements Cu and Ti presents wavy. Furthermore, the SEM–EDS line analysis of brazing interfacial microstructure of Ti/Cu CMT butt joint indicated that Al element was enriched in the brazing interface between Ti base metal and the weld metal. Base on Fig. 12(a–b), it is also found that the thickness of IMCs layer in interface zone C and D was different. Ref. [6] also presented the thickness of IMCs layer was different during different temperature and reaction time. Though the thickness of IMCs layers with good reaction bonding reached 100 μm, the satisfied Cu–Ti welded joints were not fractured at the Cu–Ti IMCs layer, which was concerned with two aspects. On the one hand, the Cu–Ti IMCs layer between weld metal and Ti sheet was not straight, but curve, thus, the larger area IMCs layer with curved shape was not perpendicular to the tensile normal stress. On the contrary, the fracture was produced at the soften Cu HAZ due to higher tensile stress.

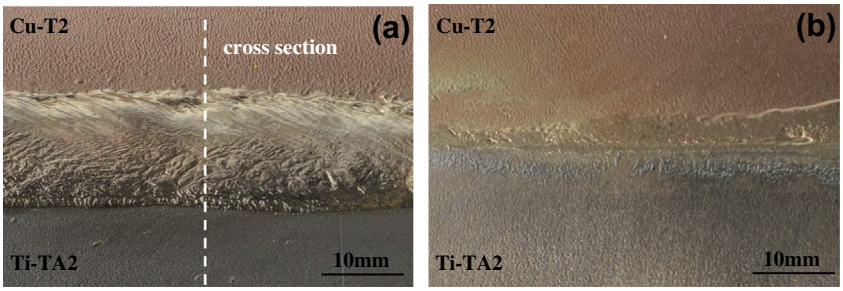

Fig. 7. Weld appearance of the Ti/Cu CMT butt *joint III* (T2–30, TA2–30) at the wire feed speed of 9.5 m/min: (a) front side, and (b) back side.

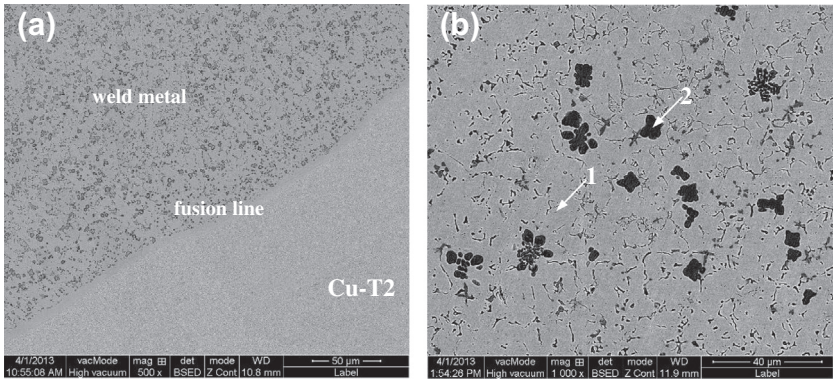

Fig. 9. Microstructures of fusion welding joint: (a) fusion line zone A in Fig. 8, and (b) weld metal zone B in Fig. 8.

Table 4
EDS results of weld metal from Fig. 9(b) (at%).

Points in Fig. 9(b)	Ti	Cu	Al	Ni	Fe	Phase
1	1.4	83.5	13.2	1.0	0.9	α-Cu solid solution
2	26.2	24.5	22.1	15.0	12.1	Ti–Cu–Al–Ni–Fe multi-phase

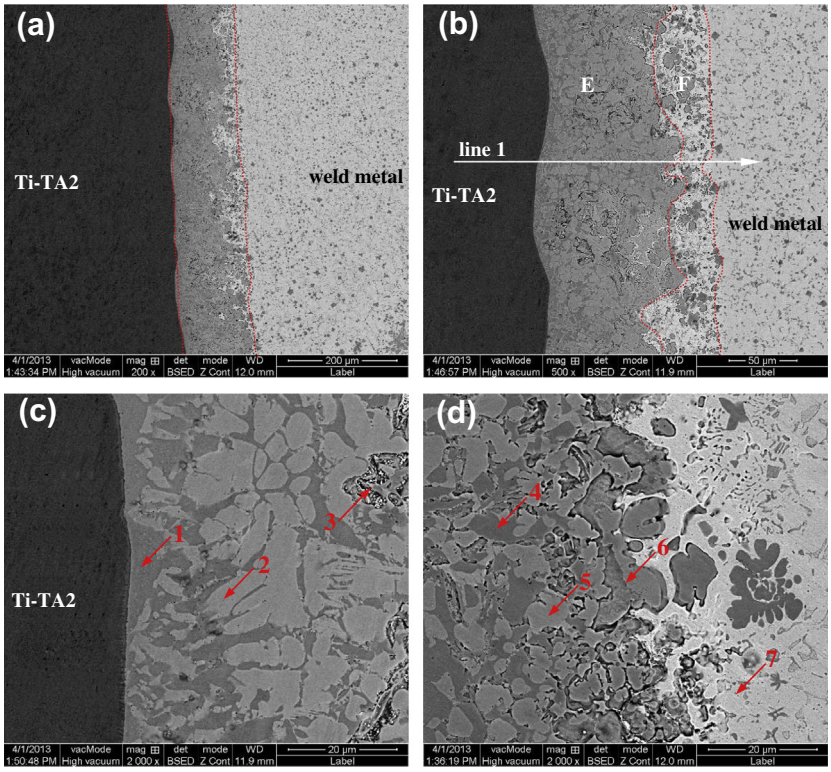

Fig. 10. Microstructures of middle groove part of brazing interface C: (a) Zone C in Fig. 8, (b) higher magnification of zone C in Fig. 8, (c) higher magnification of zone E in (b), and (d) higher magnification of zone F in (b).

4. Discussion

4.1. Crystallization behavior of Ti/Cu CMT welding–brazing joint

According to the analysis of preceding context, microstructures of fusion welding joint consists of α-Cu solid solutions and Cu–Al–Ti–Fe–Ni multi-phases distributed at the grain boundaries. And the solidification process of fusion welding joint may be described as following:

(i) During melting and mixing of ERCuNiAl filler metal and Cu alloy for CMT welding–brazing, partial Cu base metal is molten in fusion zone. Thus, the metals in this zone are a semi-molten state mixed by solid and liquid metal, as shown in Fig. 13(a). At the same time, Ti atoms diffuse into weld pool.
(ii) With decreasing of temperature, preferential heterogeneous nucleations of grains are carried out at the solid/liquid interface. Because the highest temperature gradient is produced along the direction perpendicular to the solid/liquid

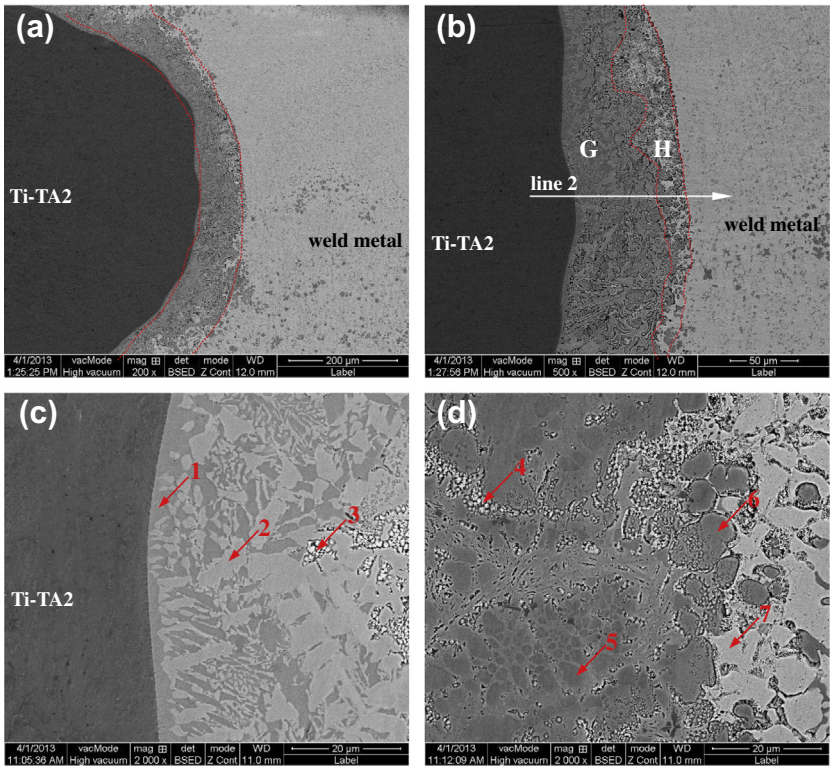

Fig. 11. Microstructures of the root groove surface of brazing interface D: (a) Zone D in Fig. 8, (b) higher magnification of zone D in Fig. 8, (c) higher magnification of zone G in (b), and (d) higher magnification of zone H in (b).

Table 5
EDS results of brazing interface zone C from Fig. 10 (at%).

Points in Fig. 10	Ti	Cu	Al	Ni	Fe	Possible phase
1	62.9	31.9	4.0	0.8	0.4	Ti_2Cu
2	48.6	39.4	5.4	2.7	4.0	TiCu
3	13.7	80.7	3.9	0.9	0.7	α-Cu solid solution
4	57.4	34.8	6.6	1.0	0.2	Ti_2Cu
5	44.8	40.5	6.1	3.0	5.6	TiCu
6	25.5	49.1	17.9	4.4	3.1	$AlCu_2Ti$
7	1.5	85.8	11.2	0.8	0.7	α-Cu solid solution

Table 6
EDS results of brazing interface zone D from Fig. 11 (at%).

Points in Fig. 11	Ti	Cu	Al	Ni	Fe	Possible phase
1	58.8	33.1	5.3	1.4	1.5	Ti_2Cu
2	46.8	40.3	5.6	2.7	4.5	TiCu
3	16.5	77.0	3.9	1.4	1.1	α-Cu solid solution
4	11.9	82.4	4.3	0.8	0.6	α-Cu solid solution
5	43.6	39.5	7.0	5.5	4.4	TiCu
6	24.8	52.5	16.4	3.6	2.6	$AlCu_2Ti$
7	5.9	88.3	5.0	0.5	0.3	α-Cu solid solution

interface, α-Cu gains grow rapidly along this direction, which induces formation of the coarse columnar crystal structures. The liquid filler metal wets the solid Ti surface, and form the IMCs layer, as shown in Fig. 13(b).

(iii) With further decreasing of the temperature, the degree of supercooling increases in the weld pool. Thus, homogeneous nucleation starts to proceed and weld pool begins to crystallize. As a joining method with filler wire, weld pool is stirred sharply during the solidification. For this reason, the temperature distribution is uniform. Hence, α-Cu grains are

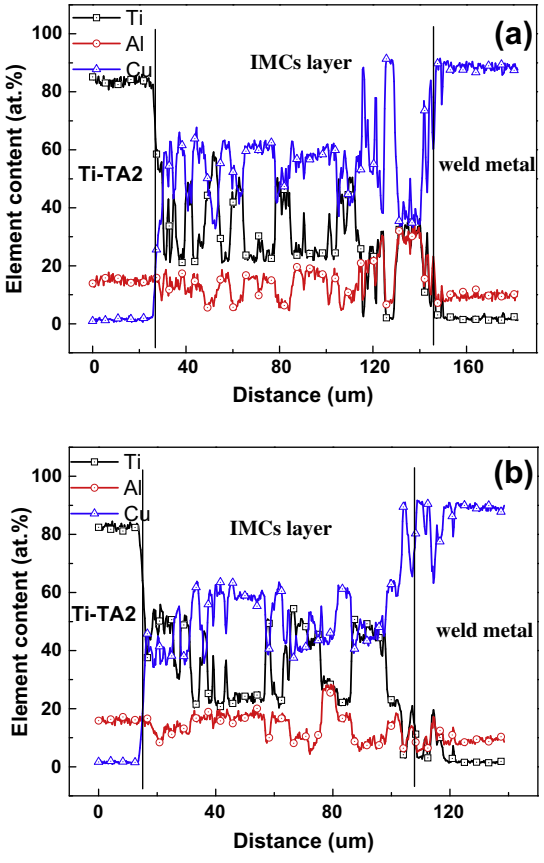

Fig. 12. Line analysis of brazing interface: (a) *line 1* marked in Fig. 10(b), and (b) *line 2* marked in Fig. 11(b).

precipitated from liquid phase firstly, and the Al, Ti, Fe and Ni atoms gather to liquid phase, and then Cu–Al–Ti–Fe–Ni multi-phases are formed, as shown in Fig. 13(c).

(iv) After liquid metal solidifies completely, fusion welding joint is formed, as shown in Fig. 13(d).

The wire and Cu sheet were molten and mixed to form a fusion welding joint. Moreover, Ti sheet was little molten or maintain solid, and the liquid filler metal wetted and spread on the Ti sheet to form a brazing joint. Then, welding–brazing joints were produced between Ti and Cu. Song et al. [10,11] reported that sheets of Al 5A06 and steel AISI 321 were butt-joined by melting the Al sheet alone using TIG welding–brazing process, which was similar to the obtained results in this study. The studies carried out on laser welding–brazing of Ti to Al [12] and electron beam self-melting brazing of Ti to Cu [13] also found similar results.

4.2. Mechanism of brazing interfacial reaction

The brazing joint is formed by interfacial reaction between liquid filler metal and solid Ti base metal. The interfacial reaction process may be described as following:

(i) The liquid filler metal wets and spreads at the solid Ti surface in the wetting process of liquid flux film. Ti atoms dissolve into the liquid filler metal and subsequently diffuse in the liquid filler metal. Because enthalpy of mixing of Al in Ti is −119 kJ/mole more negative than −34 kJ/mole of Al in Cu [26], Al atoms continually aggregate to the brazing interface close to Ti base metal from weld pool, as shown in Fig. 14(a).

(ii) In the solidifying process of brazing interface and with rich content of Ti close Ti base metal, the Ti_2Cu phase with a high melting point of 1005 °C, nucleates and grows up in the interface between Ti base metal and liquid filler metal, as shown in Fig. 14(b).

(iii) As the decreasing of the temperature and Ti content, the TiCu phase with a melting point of 982 °C, nucleates and grows up. Heterogeneous nucleation is achieved easily at solid/liquid interface, as shown in Fig. 14(c).

(iv) With further extending to weld pool, when the contents of Al atoms in the liquid filler metal gathered to enough level, ternary IMC $AlCu_2Ti$ phases begin to crystallize at the interface. After liquid metal solidifies completely, the welding–brazing joint is formed, as shown in Fig. 14(d).

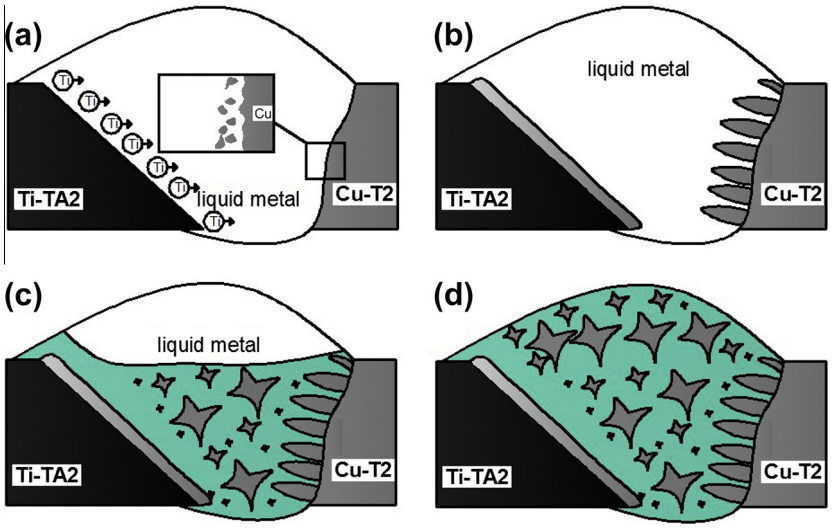

Fig. 13. Crystallization behavior of Ti/Cu CMT welding–brazing joint: (a) formation of weld pool and diffusion of element Ti, (b) formation of columnar crystal zone and IMCs layer, (c) solidification of the seam, and (d) formation of the joint.

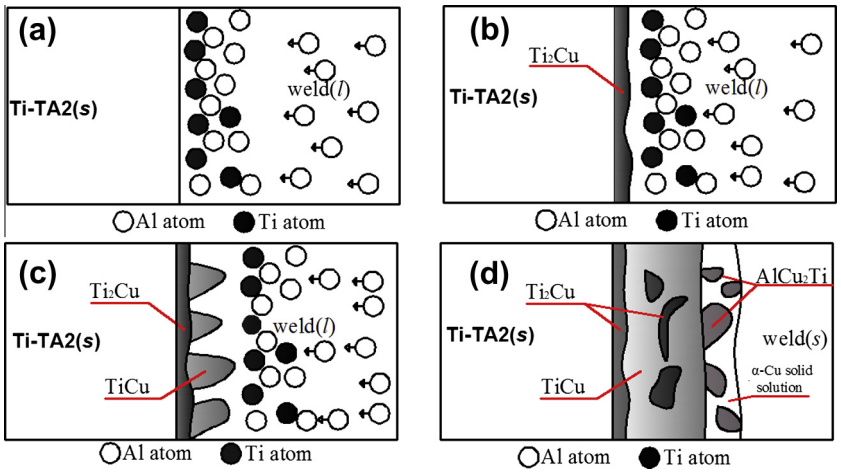

Fig. 14. Growth process of the IMCs layers during Ti/Cu CMT welding–brazing: (a) dissolution and diffusion of Ti and aggregation of Al in the interface, (b) nucleation and growth of Ti_2Cu, (c) nucleation and growth of TiCu, and (d) nucleation and growth of $AlCu_2Ti$ and solidification of fusion brazing joint.

In short, with the decreasing of Ti content and temperature, and the diffusion of Al, IMCs layers including Ti_2Cu, TiCu, $AlCu_2Ti$ phases between Ti base metal and weld metal were formed in order. Shiue et al. [2,3] reported infrared brazing commercially pure titanium and oxygen free copper. When using pure Ag as filler metal, Ti_2Cu and TiCu phases were observed near Ti base metal. While using pure 95Ag–5Al as filler metal, the zone near Ti base metal consisted of Ti_2Cu and $AlCu_2Ti$ phases. The results were seen to be in agreement with the obtained results in this study.

5. Conclusions

According to the study on cold metal transfer welding–brazing of titanium to copper, the followed conclusions can be summarized:

(1) A satisfied Ti/Cu CMT welding–brazing butt joint was successfully obtained by CMT welding–brazing with ERCuNiAl copper wire as filler metal when wire feed speed was controlled at 9.0 m/min –9.5 m/min (I_w = 210–223 A).
(2) The welding joint was formed at Cu alloy side, while brazing joint was formed in titanium alloy side, i.e. welding–brazing joints were produced between Ti TA2 and Cu T2.
(3) The thickness of the IMCs layer was ununiformed: 117–129 μm in middle groove surface, and 80–100 μm in root groove surface. The IMCs layers at the brazing interface mainly consisted of Ti_2Cu, TiCu and $AlCu_2Ti$ orderly from the Ti base metal to the weld metal.
(4) At the optimized welding variables, the type of the groove and the IMCs layer of Cu–Ti brazing interface have no effects on the tensile load of the joints. The sufficient strength at interlamellar layers makes the fracture move to HAZ of Cu base metal. In this case, the tensile load of the joints is only concerned about the soften degree of Cu HAZ. The Cu/Ti CMT butt joints at the optimized welding variables can reach tensile load of 5.10 kN, and fractured in Cu HAZ.

Acknowledgements

This research work was financially supported by National Nature Science Foundation of China (No. 51265028), and the rose willow outstanding individual programs of Lanzhou university of Technology.

References

[1] Li YJ, Wang J, Liu P. Weld of dissimilar metals and their applications in industries. Beijing: Chemical Industry Press; 2003.
[2] Shiue RK, Wu SK, Chan CH. The interfacial reactions of infrared brazing Cu and Ti with two silver-based braze alloys. J Alloy Compd 2004;372:148–57.
[3] Shiue RK, Wu SK, Chan CH. Infrared brazing Cu and Ti using a 95Ag–5Al braze alloy. Metall Mater Trans A 2004;35A:3177–86.
[4] Liu W, Chen GQ, Zhang BG, Feng JC. Analysis of structure and growth of QCr0.8/TC4 welded reaction layer by electron beam welding. Trans China Weld Inst 2008;29:85–8.
[5] Liu W, Zhang BG, He JS, Zhao HS. Microstructure and performance of dissimilar joint QCr018/TC4 welded by uncentered electron beam. Rare Metal 2007;26:344–8.
[6] Aydin K, Kaya Y, Kahraman N. Experimental study of diffusion welding/bonding of titanium to copper. Mater Des 2012;37:356–68.
[7] Kimura M, Saitoh Y, Kusaka M, Kaizu K, Fuji A. Effect of friction pressure on joining phenomena of friction welds between pure titanium and pure copper. Sci Technol Weld Joining 2011;16(5):392–8.
[8] Kim SY, Jung SB, Shur CS. Mechanical properties of copper to titanium joined by friction welding. J Mater Sci 2003;38:1281–7.
[9] Kahraman N, Gülenc B. Microstructural and mechanical properties of Cu–Ti plates bonded through explosive welding process. J Mater Process Technol 2005;169:67–71.
[10] Song JL, Lin SB, Yang CL, Ma GC, Liu H. Spreading behavior and microstructure characteristics of dissimilar metals TIG welding–brazing of aluminum alloy to stainless steel. Mater Sci Eng, A 2009;509:31–40.
[11] Song JL, Lin SB, Yang CL, Fan CL. Effects of Si additions on intermetallic compound layer of aluminum-steel TIG welding–brazing joint. J Alloy Compd 2009;488:217–22.
[12] Chen SH, Li LQ, Chen YB, Huang JH. Joining mechanism of Ti/Al dissimilar alloys during laser welding–brazing process. J Alloy Compd 2011;509:891–8.
[13] Zhang BG, Wang T, Chen GQ, Feng JC. Microstructure and mechanical property of electron beam self-melting brazing joint of titanium alloy to chromium bronze. Rare Metal Mater Eng 2012;41(1):129–33.
[14] Yang XR. Welding of steel and aluminum. Aeronaut Manuf Technol 2004;12:96–7.
[15] Yang XR. CMT cold metal transfer process. Electr Weld Mach 2006;36(6):5–7.
[16] Cao R, Yu G, Chen JH, Wang PC. Cold metal transfer joining aluminum alloys-to-galvanized mild steel. J Mater Process Technol 2013;213:1753–63.
[17] Zhang HT, Feng JC, He P, Zhang BB, Chen JM, Wang L. The arc characteristics and metal transfer behaviour of cold metal transfer and its use in joining aluminium to zinc-coated steel. Mater Sci Eng, A 2009;499:111–3.
[18] Cao R, Sun JH, Chen JH. Mechanisms of joining aluminium A6061–T6 and titanium Ti–6Al–4V alloys by cold metal transfer technology. Sci Technol Weld Joining 2013;18(5):425–33.
[19] ISO 4136–2012. Destructive tests on welds in metallic materials-Transverse tensile test, 2012.
[20] ISO 9015–1: 2001. Hardness test methods on welded joints, 2001.
[21] Li LB, Sun YF. Handbook of metal materials. Beijing: China Machine Press; 2011.
[22] Tetsui T. Effects of brazing filler on properties of brazed joints between TiAl and metallic materials. Intermetallics 2001;9:253–60.
[23] Yu J, Wu BW, Zheng SB, Wang KH, Zhou Q. Microstructures and properties of copper-steel welded joint by twin wire welding. Rare Metal Mater Eng 2011;40(S4):302–5.
[24] Murray JL. The Cu–Ti (copper–titanium) system. J Phase Equilib 1983;4(1):81–95.
[25] Villars P, Prince A, Okamoto H. Handbook of ternary alloy phase diagrams. ASM International Metals Park; 1995.
[26] Niessen AK, de Boer FR, Boom R, de Châtel PF, Mattens WCM, Miedema AR. Model predictions for the enthalpy of formation of transition metal alloys II. CALPHAD 1983;7(1):51–70.